ADVANCED FUNCTIONAL MATERIALS

DOI: 10.1002/adfm.200800454

Perfluorooctyl Bromide Polymeric Capsules as Dual Contrast Agents for Ultrasonography and Magnetic Resonance Imaging

By *Emilia Pisani, Nicolas Tsapis, Belfor Galaz, Mathieu Santin, Romain Berti, Nicolas Taulier, Erol Kurtisovski, Olivier Lucidarme, Michèle Ourevitch, Bich Thuy Doan, Jean Claude Beloeil, Brigitte Gillet, Wladimir Urbach, S. Lori Bridal,* and *Elias Fattal**

Polymeric capsules with a thick shell made of biodegradable and biocompatible polymer and a liquid core of perfluorooctyl bromide (PFOB) were evaluated for stability as well as for ultrasound and magnetic resonance imaging (MRI) contrast enhancement. The method of preparation allows the mean capsule diameter to be regulated between 70 nm and 25 μm and the capsule thickness-to-radius ratio from 0.25 to 0.54. Capsule diameter remains stable at 37 °C in phosphate buffer for at least 4 and 6 h for nanocapsules and microcapsules, respectively. The *in vitro* ultrasound signal-to-noise ratio (SNR) was measured from 40 to 60 MHz for 6 μm and 150 nm capsules: the SNR increases with capsule concentration up to 20–25 mg mL^{-1}, and then reaches a plateau that depends on capsule diameter (13.5 ± 1.5 dB for 6 μm and 6 ± 2 dB for the 150 nm capsules). The ultrasound SNR is stable for up to 20 min for microcapsules and for several hours for nanocapsules. For nanocapsules, the thinner the shell, the larger the SNR and the more compressible the capsules. Nanocapsule suspensions imaged *in vitro* with a commercial ultrasound imaging system (normal and tissue harmonic imaging modes, 7–14 MHz probe) were detected down to concentrations of 12.5 mg mL^{-1}. Injections of nanocapsules (200 μg ml^{-1}) in mice *in vivo* reveal that the initial bolus passage presents significant ultrasound enhancement of the blood pool during hepatic imaging (7–14 MHz probe, tissue harmonic imaging mode). ^{19}F-MRI images were obtained *in vitro* at 9.4T using spin-echo and gradient echo sequences and allow detecting nanocapsules in suspension (50 mg mL^{-1}). In conclusion, these results show initial feasibility for development of these capsules toward a dual-modality contrast agent.

1. Introduction

Research developing molecularly targeted medical imaging and therapy has increased tremendously in recent years.[1] The principle is based on the detection of probes providing imaging contrast that can be targeted to specific molecular markers. The potential of molecularly targeted contrast agents to elucidate molecular processes, to provide specific diagnosis and to help to target therapy has been demonstrated.[2] Although, positron emission tomography (PET) is the most well-established molecular imaging technique and provides the highest sensitivity for probe detection, ultrasound and

[*] Prof. E. Fattal, Dr. E. Pisani, Dr. N. Tsapis
Univ Paris Sud, UMR CNRS 8612
IFR 141, Châtenay-Malabry (France)
E-mail: elias.fattal@u-psud.fr

Dr. E. Pisani, Dr. N. Tsapis, Prof. E. Fattal
CNRS, UMR 8612, IFR 141
Châtenay-Malabry (France)

B. Galaz, M. Santin, R. Berti, Dr. N. Taulier, Dr. E. Kurtisovski, Prof. W. Urbach, Dr. S. L. Bridal
UPMC Univ Paris 06, UMR 7623
LIP, 75005, Paris (France)

B. Galaz, M. Santin, R. Berti, Dr. N. Taulier, Dr. E. Kurtisovski, Prof. W. Urbach, Dr. S. L. Bridal
CNRS, UMR 7623
Laboratoire d'Imagerie Paramétrique
75006, Paris (France)

B. Galaz
Departamento de Física
Universidad de Santiago de Chile (USACH)
Santiago (Chile)

Dr. O. Lucidarme
UPMC Univ Paris 06
UMR-S 678 INSERM
LIF, 75005, Paris (France)

Dr. O. Lucidarme
INSERM, U678
Laboratoire d'Imagerie Fonctionnelle
75013, Paris (France)

M. Ourevitch
Univ Paris Sud, UMR CNRS 8076, BioCIS
IFR 141, Châtenay-Malabry (France)

Dr. B. T. Doan, Dr. J. C. Beloeil
CNRS UPR 4301
Centre de Biophysique Moléculaire
Orléans (France)

Dr. B. Gillet
CNRS UPR 2301
ICSN
Gif sur Yvette (France)

[**] Authors would like to thank D. Jaillard and J. Degrouard (CCME, Orsay) for TEM experiments, A. Allavena-Valette (CECM, Vitry sur Seine) for access to the SEM facility, V. Nicolas (IFR 141, ITFM) for confocal microscopy, P. Laugier for fruitful discussions, L. Harivardhan Reddy for help with animals, and G. Barratt for carefully proofreading the manuscript. Authors acknowledge financial support from ANR (Agence Nationale de la Recherche, NT05-3_42548), in particular for fellowships to E.P. and N.T. This study was funded in part by the EC – FP6-project DiMI, LSHB-CT-2005-512146.

magnetic resonance imaging (MRI) are highly attractive modalities that avoid exposition to ionizing radiations[3,4] and provide superior spatial resolution.[5,6] Ultrasound, furthermore, allows real-time temporal resolution.

The list of characteristics desired by imaging scientists for molecular contrast agents is long. Agents need to provide very target-specific binding and sufficient stability in the circulation to allow strong and selective accumulation. They need to be non-toxic and sensitively detectable. Ideally, they should be suitable to carry and deliver therapeutic payload. Highly controlled physical characteristics should help obtain more uniform kinetic behavior and contribute to the implementation of quantitative detection techniques. Finally, depending upon the biological target's compartment, agent size should be tailored either to limit circulation to the vascular space (micrometric but less than $\sim$7 μm) or to allow passage beyond the endothelium (nanometric).

For both ultrasound and MRI, contrast agents are currently used to improve visualization of the microvasculature. Commercial ultrasound contrast agents (UCAs), consisting of encapsulated gas microbubbles injected intravenously, improve visualization of the vascular tree, but their limited stability hampers their use as molecularly targeted agents. Several reports have proposed the use of polymers to increase the stability of UCAs, since polymeric shells would resist dissolution and acoustic pressures better than the monomolecular layers of lipids or proteins usually stabilizing commercial UCAs.[7–10] Moreover, because of their high difference of density with air and their poor solubility in water, perfluorocarbons have been shown to increase both the stability and the echogenicity of UCAs.[11] Lanza et al.[12] as well as Wickline et al.[13] have shown that nanoemulsions of liquid perfluorocarbons in water have interesting ultrasound properties similar to gaseous perfluorocarbons, particularly at high frequencies (>15 MHz), and they suggest that such agents would be useful for small animal imaging.

In addition to their ultrasound properties, perfluorinated molecules have applications for MRI. Indeed, although ^{1}H (H_2O) MRI is most frequently performed, ^{19}F MRI would present several advantages. ^{19}F has a gyromagnetic ratio nearly equivalent to the proton, a spin ½ nucleus and 100% natural abundance. Moreover, the fluorine present in the body is mostly in the form of solid fluoride in bones and teeth[14] and since endogenous fluorine has a very short T2 relaxation time[14] the resulting signal is below the limits of NMR detection in most biological systems. Therefore, exogenously administered fluorinated compounds can be observed without interference from background signal. Several studies have already demonstrated the interest of perfluorocarbons nanoemulsions for ^{19}F MRI.[15–18] In emulsions however, fluorinated molecules are easily accessible to other substances present *in vivo* such as oxygen[19] and since ^{19}F is exquisitely sensitive to perturbations in its microenvironment, chemical shifts may occur.[20]

It is clear from the literature that both ultrasound and MRI contrast agents possess certain common requirements and that the development of polymeric capsules of perfluoroctyl bromide could provide dual imaging with these techniques. Indeed, a biodegradable[21] and biocompatible[22] polymer shell would improve the stability of the capsules compared with UCAs stabilized by a monomolecular layer, while the perfluorocarbon core could provide echogenicity.[23] Polymeric capsules of perfluorocarbons may as well protect fluorinated molecules and prevent any unpredicted shift due to the chemical microenvironment of these molecules during MRI.

We present briefly here the preparation method as well as the main physical features of novel nano/microcapsule agents. These biocompatible capsules have been characterized previously in terms of size, polydispersity, morphology, and thickness.[24] Capsule diameter can be precisely tuned between 70 nm and 25 μm and capsule thickness to radius ratio can be adjusted between 0.25 and 0.54. In addition, capsules can be easily freeze-dried without change of their physical features. The aim of this article is to characterize the *in vitro* stability of these agents, to investigate the effect of shell thickness on ultrasound properties and to explore their potential to provide ultrasound and magnetic imaging enhancement. In this work, stability in suspension was assessed for both micro- and nanocapsules using laser diffraction or light scattering. *In vitro* ultrasound measurements (40–60 MHz) were used to characterize the ultrasound signal-to-noise ratio (SNR) as a function of agent size, concentration, and time since resuspension. The effect of modifying shell thickness on compressibility and ultrasound SNR was also investigated. Suspensions of capsules were imaged *in vitro* and in mice *in vivo* with a medical ultrasound imaging system (7–14 MHz). The ^{19}F-MRI SNR of nanocapsule suspensions as a function of concentration was measured using high resolution ^{19}F spectroscopy as well as capsule spin–spin (T1) and spin-echo (T2) relaxation times. Finally, capsules suspensions were imaged *in vitro* with an MRI scanner at 9.4T using either spin-echo or gradient echo sequences.

2. Results and Discussion

Nanocapsules (150 nm diameter) and microcapsules (6 μm diameter) of PLGA with a perfluorooctyl bromide (PFOB) core were prepared as previously described in Ref.[24] by a modification of the emulsion–evaporation process, derived from the techniques described by Loxley and Vincent[25] for the preparation of poly(methylmethacrylate) microcapsules with liquid cores. Previous work has demonstrated that the capsule thickness can be controlled by varying the PFOB/PLGA proportions and that the liquid PFOB core is consistently well centered.[24] Several experiments described in Ref.[24] have proved that the central cavity of the capsules contains liquid (and not gaseous) PFOB.

2.1. Physical Properties of the Capsules

Microscopy images show spherical particles with a single core.[24] Nile red added to the organic solution prior to emulsification provides specific labeling of the hydrophobic

ADVANCED FUNCTIONAL MATERIALS

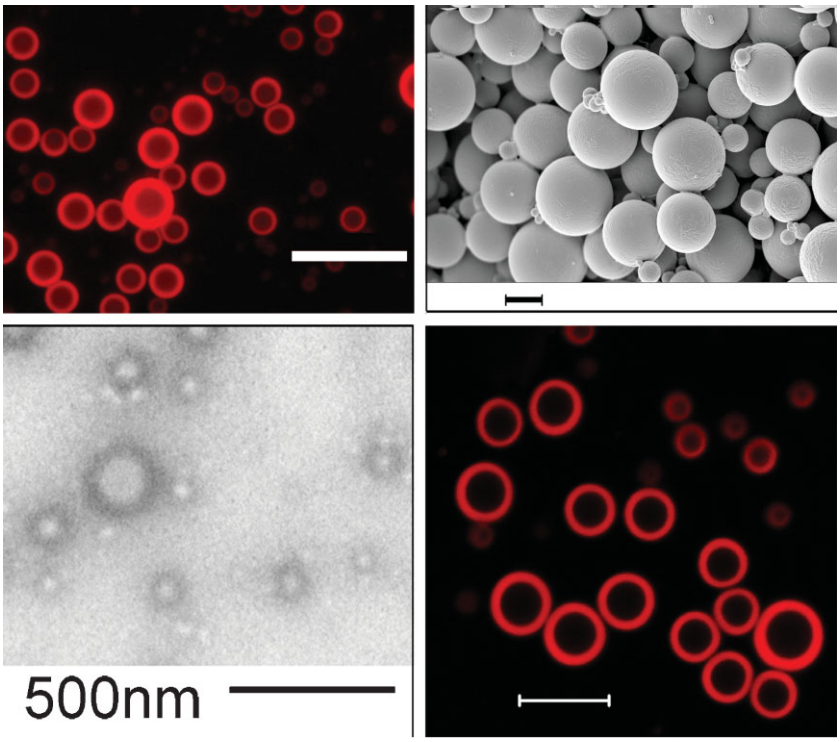

Figure 1. Top-left: Fluorescent microscopy image of a suspension of microcapsules: the polymer appears bright and the liquid perfluorocarbon appears dark (scale bar = 20 μm). Top-right: SEM images of microcapsules, they present a smooth surface (scale bar = 2 μm). Bottom-left: TEM image of typical nanocapsules: because of the difference of electronic density, the PFOB liquid core appears in gray, whereas the polymeric shell seems darker. Bottom-right: Confocal microscopy image of microcapsules prepared with 60 μL PFOB and 0.1 g PLGA (scale bar = 10 μm).

polymer capsule. Fluorescent microscopy images show spherical particles with a clear red shell of homogeneous thickness and a darker core (Fig. 1, top-left). Moreover, the different slices obtained by confocal microscopy prove that the cavities are well centered within the particles and that the shell thickness is homogeneous for each particle (Fig. 1, bottom-right). Capsules could be obtained with several perfluorocarbons[24] among which PFOB. This compound is of particular interest since no toxicity has ever been reported for this chemical.[26,27] Scanning electron microscopy (SEM) images reveal that capsules are spherical with a smooth surface (Fig. 1, top-right).

The preparation process is very versatile and capsule diameter can be controlled simply by varying the emulsification speed or the sodium cholate concentration, yielding capsules with a mean diameter between 1 and 25 μm. When emulsification is performed with an ultrasound tip within the same process, capsule size can be further reduced to form nanocapsules with a mean diameter ranging from 70 to 300 nm, as shown on the TEM image (Fig. 1, bottom-left). We have chosen to evaluate 6 ± 1.5 μm and 150 ± 30 nm capsules as typical micro- and nanocapsules. The preparation process also allows us to tune the dimensionless parameter T/R (T = capsule thickness, R = capsule radius) between 0.25 and 0.54, simply by modifying the PLGA/PFOB proportions, independently of capsule diameter. Nanospheres ($T/R = 1$) can also be obtained omitting PFOB in the formulation.

2.2. Stability

Capsules withstand freeze-drying without any modification in diameter or T/R, a key advantage for storage.[24] Capsule stability after resuspension in PBS from freeze-dried samples was assessed *in vitro* at 37 °C. Nanocapsule diameter remains stable over 4 h of incubation at 37 °C and then increases from 150 ± 30 nm to approximately 250 ± 75 nm. This may be due to polymer degradation, capsule aggregation or PFOB leakage. Microcapsule size did not vary in PBS for the 6 h incubation time of the test. These results were confirmed by fluorescent microscopy: capsule morphology was conserved for the vast majority of microcapsules (>90%) for at least for 6 h.

2.3. Ultrasound Enhancement

2.3.1. In Vitro Evaluation of Concentration and Temporal Variations (40–60 MHz)

For small animals, ultrasound imaging investigations are optimized when using high ultrasound frequencies. For this reason, as well as the fact that high frequency measurements allowed the use of small sample volumes, the acoustic efficiency of our capsules was initially assessed within the 40–60 MHz frequency bandwidth. First of all, no significant difference in contrast SNR (within an error of 1 dB) was observed between fresh and resuspended freeze-dried capsules, even 24 h after their reconstitution. Thus, the freeze-drying process does not alter capsule ultrasound properties. Specifically, we have investigated the behavior of the SNR as a function of capsule concentration up to 50 mg mL^{-1} (Fig. 2, top). For 6 μm capsules, 50 mg mL^{-1} corresponds to about 4×10^8 capsules mL^{-1}, whereas for 150 nm capsules, 50 mg mL^{-1} corresponds to about 2×10^{13} capsules mL^{-1} due to the size difference. Independently of capsule size, we observe an increase of the SNR up to 20–25 mg mL^{-1}, followed by a plateau corresponding to SNR saturation. SNR saturation has been observed in previous studies of ultrasound contrast agents:[8,9,28,29] it usually arises from multiple scattering. The plateau values depend on capsule size and are equal to 13.5 ± 1.5 dB for 6 μm capsules and to about 6 ± 2 dB for 150 nm capsules. Current theoretical models fail to predict correctly the acoustic behavior of our capsules since they were developed for bubble-based contrast agents with a thin shell.[30–33] Consequently, the shell acoustic properties and

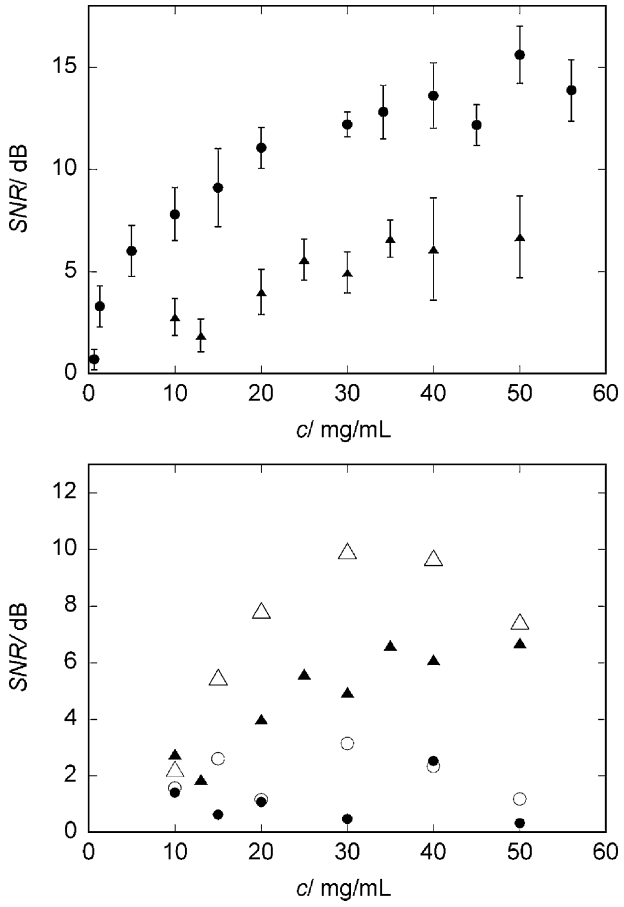

Figure 2. Top: Ultrasound SNR versus capsule concentration in water as measured in the specimen chamber at 50 MHz (T/R is 0.35, capsule median size: 6 μm (●) and 150 nm (▲)). For 6 μm capsules, 50 mg mL^{-1} corresponds to about 4×10^8 capsules mL^{-1}, whereas for 150 nm capsules, 50 mg mL^{-1} corresponds to about 2×10^{13} capsules mL^{-1}. Bottom: Ultrasound SNR versus nanocapsule concentration (median size 150 nm) for different T/R ratios: $T/R = 1$ (●), $T/R = 0.54$ (○), $T/R = 0.35$ (▲), and $T/R = 0.25$ (△). Error bars have been omitted on purpose to allow clear reading of the graph (SD ≤ 1–2 dB). Measurements were performed at least in triplicate for all experiments.

the liquid core, which are significant for our capsules, are neglected in these models. It is interesting to note that our 150 nm nanocapsules exhibit some echogenicity whereas perfluorocarbon emulsions of approximately the same size do not give any signal unless they are bound to a surface.[12,13,34–36]

For well-homogenized microcapsule suspensions, the SNR was quite stable for up to 20 min. Thereafter, microcapsule sedimentation could effect SNR measurement, however, the signal could be recovered easily by homogenizing the suspension. For nanocapsule suspensions SNR remained stable for several hours since they do not sediment. This *in vitro* stability is better than that which has been reported for other polymer-based contrast agents for which the SNR decreases drastically or disappears after only a few minutes.[7,8,37,38]

2.3.2. In Vitro Evaluation of Enhancement with Nanocapsule Thickness (40–60 MHz), Compressibility Measurements

Since SNR measurements demonstrated that nanocapsules are detectably echogenic although with a lower efficiency than microcapsules, the following experiments concentrate on nanocapsule contrast response. Indeed, the smaller the particles, the lower the possibility that they could produce pulmonary embolism *in vivo*. Moreover, nanocapsules are much more versatile than microcapsules since, due to their small size, they can be taken up by macrophages of the mononuclear phagocyte system (MPS)[39] or even undergo an enhanced permeability and retention effect in neovascularized tumors provided their surface can be pegylated.[39] The effect of capsule thickness on echogenicity was assessed for 150 nm nanocapsules. Figure 2 (bottom) presents the variation of the SNR measured at 50 MHz for different T/R ratios. $T/R = 1$ corresponds to homogeneous nanospheres of PLGA with no PFOB core. On one hand, nanospheres do not exhibit any significant signal as compared with water. The SNR obtained for nanocapsules with $T/R = 0.54$ is slightly more important. On the other hand, for $T/R = 0.35$, the SNR can reach up to $6 \pm$ dB, and up to 10 ± 2dB for $T/R = 0.25$. The thinner the shells, the higher the SNR. These results are closely related to compressibility results: as the absolute shell thickness decreases, nanocapsules become more compressible (Fig. 3) and therefore backscatter ultrasonic waves more efficiently.

2.3.3. In Vitro Ultrasound Imaging

Capsule suspensions were imaged *in vitro* with a commercial ultrasound imaging system (7.5 MHz, L40 clinical ultrasound probe, Sonoline Elegra, Siemens, Germany). Images obtained at the same machine settings to compare the background gray-scale level in a water-filled silicon tube with contrast enhancement observed when the tube was filled with nanocapsule suspensions (150 nm diameter, $T/R = 0.35$) are presented in Figure 4. Enhancement was evaluated as a

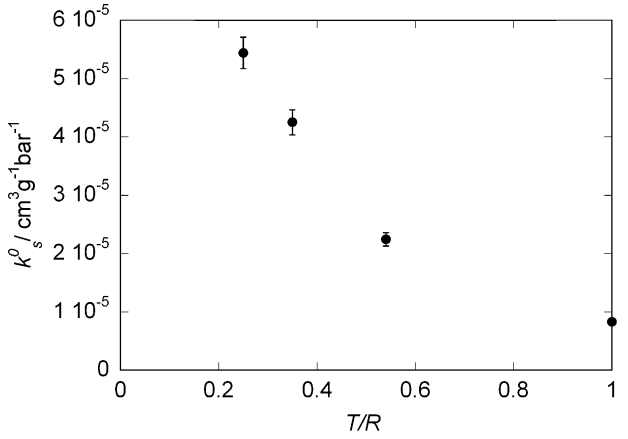

Figure 3. Nanocapsule adiabatic compressibility as a function of absolute thickness T/R. The higher k^0, the more compressible the nanocapsules.

ADVANCED FUNCTIONAL MATERIALS

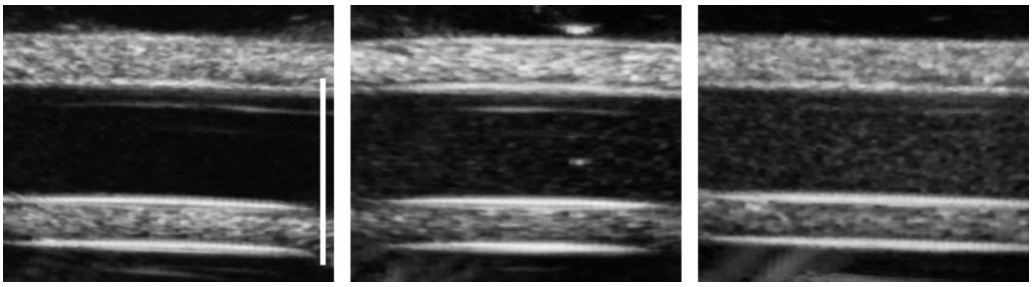

Figure 4. Ultrasound images obtained *in vitro* in nonlinear mode (THI). Water in a silicone tube appears dark whereas horizontal tube walls are clearly visible (left). 150 nm capsules produce a significant enhancement that allows them to be distinguished from pure water (center: 12.5 mg mL^{-1}, right: 50 mg mL^{-1}). The scale bar represents 1 cm.

function of capsule concentration (from 5 to 50 mg mL^{-1}). Nanocapsule suspensions appear brighter than background when imaged both in the normal mode (not shown here) and in THI mode (Fig. 4, center and right). The contrast enhancement could be distinguished from the background down to a concentration of 12.5 mg mL^{-1}. Thus, contrast enhancement is confirmed at lower ultrasound frequencies within the clinical imaging range. In addition, the signal is quite stable with time. Detection of nanocapsules in nonlinear imaging mode could imply that nonlinear response is present. However, this is somehow surprising since ultrasound studies of perfluorocarbon emulsions have shown that small emulsion droplets (250 nm) do not exhibit any nonlinear effect at clinical frequencies.[40] In order to observe a nonlinear signal, other authors have used larger droplets (>450 nm) and higher frequencies (>15 MHz).[35,40] Our results further confirm that the polymeric shell of our capsules plays an important role for their ultrasound properties, as confirmed by compressibility measurements. Further investigation is necessary to determine if capsules do indeed respond nonlinearly or not.

2.3.4. In Vivo Ultrasound Imaging

Figure 5 presents typical ultrasound images of the liver of a mouse acquired *in vivo*. Initially, the larger vessels within the liver and the inferior vena cava appeared dark (Fig. 5, top). After nanocapsule injection (200 μL of a 50 mg mL^{-1} suspension; 150 nm diameter, $T/R = 0.35$), vessels presented significant enhancement (Fig. 5, bottom). The enhancement only lasted a few seconds. Similar enhancement was observed in the three mice included in this trial. The enhancement disappearance may have resulted from the rapid dilution of the bolus in the total blood volume (leading to a final concentration of approximately 2 mg mL^{-1} which is well below concentrations detected *in vitro*). The concentration of the capsules in circulation would be further reduced as a function of time due to uptake in the MPS since the injected capsules were not stealth.[39] Although observation was continued for 30 min, no significant enhancement above the base-line echogenicity was observed in the hepatic parenchyma. Injections were well tolerated by the mice. To conclude, these experiments demonstrate ultrasound enhancement of the blood pool *in vivo* as long as capsules were highly concentrated. These nanocapsules are therefore good candidates for blood pool contrast agents and could potentially be adapted for targeted imaging provided nanocapsules are long circulating and functionalized with specific ligands.

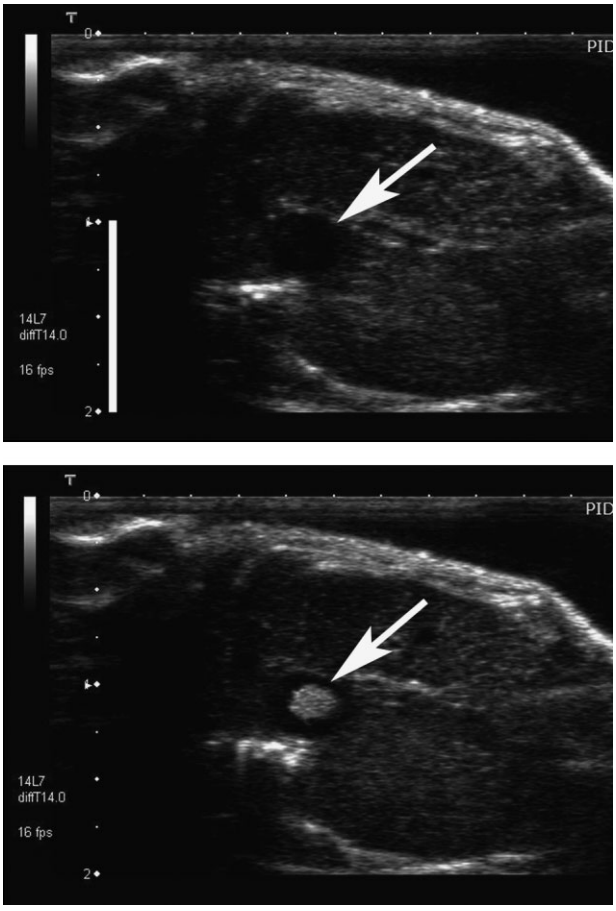

Figure 5. Ultrasound images of mouse liver obtained in THI mode before (top) and after a 200 μL injection of a 50 mg mL^{-1} suspension of 150 nm diameter capsules. The inferior vena cava (noted by an arrow) appears dark in the center of the top image, and presents significant enhancement after capsule injection (bottom). The scale bar represents 1 cm.

2.4. *In Vitro* ^{19}F magnetic Resonance Spectroscopy and Imaging

In addition to their ultrasonic properties, our capsules may also provide contrast for ^{19}F MRI. The ^{19}F spectrum of pure PFOB is characterized by seven peaks (not shown). The most intense one corresponds to the CF_3 chemical group (chemical shift of 83.4 ppm). This chemical shift is not modified when PFOB is encapsulated within PLGA capsules, demonstrating that PFOB does not interact with PLGA and is protected from molecules located outside the capsules. The SNR was measured on the CF_3 peak and increases with capsule concentration (Fig. 6, top). Even for a capsule concentration as low as 5 mg mL^{-1}, the SNR is around 10, enough to allow detection of capsules when administered *in vivo* since the fluorine concentration in the body is almost nil. T1 measurements performed on pure PFOB and PFOB nanocapsules ($c = 5$ and 10 mg mL^{-1}) give T1 $= 1.25 \pm 0.06$ s, independently of capsule concentration or whether PFOB is pure or encapsulated. These results further confirm that PFOB does not interact with PLGA and that encapsulation does not modify its magnetic properties.

Pure PFOB can be easily imaged in 8 min (Fig. 6, bottom-A, inset). Images were obtained in 8 and 34 min with 150 nm capsules in suspension ($c = 50$ mg mL^{-1}, Figure 6, bottom-A and bottom-B) respectively. Images were obtained using either a gradient echo sequence or a spin-echo sequence (not shown). Images obtained in 34 min were clearly better resolved than those obtained in 8 min. These imaging times are of the same order as those used by other groups for ^{19}F MRI[16,18] although, due to complexity of the PFOB spectrum, frequency-selective impulsions were required in our case. The apparent T2 values of the CF_3 signal remain unchanged when PFOB is encapsulated confirming the relative stability of the magnetic properties of PFOB after encapsulation: 322 ± 30 ms was found for pure PFOB and 312 ± 30 ms for 10 mg mL^{-1} nanocapsules. As a conclusion, in addition to their ultrasound properties, nanocapsules have a good potential as ^{19}F MRI contrast agents.

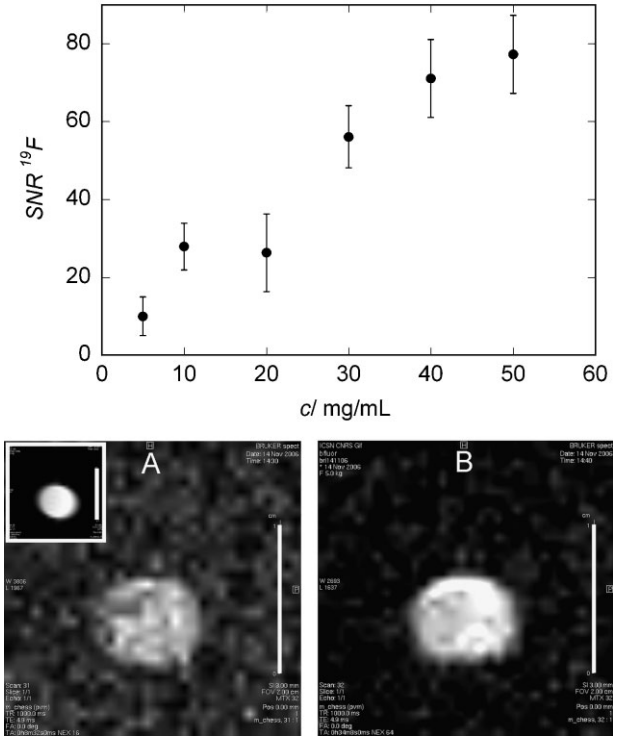

Figure 6. Top: ^{19}F spectroscopy SNR versus capsule concentration in water ($T/R = 0.35$, capsule diameter = 150 nm). Bottom: ^{19}F MRI spin-echo images of pure PFOB (A, inset, 8 min) and 150 nm capsules suspended in water (50 mg mL^{-1}: A, 8 min; B, 34 min). Scale bars represent 1 cm.

3. Conclusion

We have developed a versatile process for obtaining nano/microcapsules with a single core of liquid PFOB within a polymeric shell of PLGA of homogeneous thickness. The method of preparation allows the mean capsule diameter to be regulated between 70 nm and 25 μm and the capsule thickness-to-radius ratio from 0.25 to 0.54. The *in vitro* ultrasound SNR measured from 40 to 60 MHz for 6 μm and 150 nm capsules increases with capsule concentration up to 20–25 mg mL^{-1}, and then reaches a plateau that depends on capsule diameter (13.5 ± 1.5 dB for 6 μm and 6 ± 2 dB for the 150 nm capsules). Capsules are more stable than most polymer-based UCAs, in terms of diameter or *in vitro* ultrasound contrast enhancement. Nanocapsule shell thickness appears to be an important parameter for ultrasound contrast enhancement: the thinner the shell, the larger the SNR and the more compressible the capsules. Nanocapsule suspensions imaged *in vitro* with a commercial ultrasound imaging system (normal and tissue harmonic imaging (THI) modes, 7–14 MHz probe) were detected down to concentrations of 12.5 mg mL^{-1}. Injections of nanocapsules in mice *in vivo* reveal that the initial bolus passage presents significant ultrasound enhancement of the blood pool during hepatic imaging (14 MHz, THI mode). Finally, ^{19}F-MRI images of nanocapsules (50 mg mL^{-1}) were easily obtained in up to 34 min *in vitro* at 9.4T using spin-echo and gradient echo sequences. The ability to detect these novel contrast agents with two different imaging modalities indeed invests them with considerable potential. In the future, pegylation of the capsule surface could be considered to avoid liver accumulation and to take advantage of the enhanced permeation and retention effect to passively target tumors. Furthermore, capsule functionalization with specific ligands will allow targeting specific tissues, opening the way to molecular imaging with these dual contrast agents. Such a specific distribution would increase locally nanocapsule concentration and lower the dose required for imaging.

ADVANCED FUNCTIONAL MATERIALS

4. Experimental

Materials: Poly(lactide-*co*-glycolide) Resomer RG502 (PLGA) was provided by Boehringer-Ingelheim (Ingelheim am Rhein, Germany). Polyvinyl alcohol (PVA) (MW 30 000–70 000, 89% hydrolyzed), sodium cholate (denoted SC), and Nile Red were purchased from Sigma–Aldrich (L'Isle d'Abeau Chesnes, Saint-Quentin Fallavier, France). PFOB was a gift from Alliance Pharmaceuticals (Wiltshire, UK). Water was purified using a Milli-Q system from Millipore (France). Methylene chloride RPE-ACS 99.5% was provided by Carlo Erba Reactifs (Chaussée du Vexin, Val de Reuil, France).

Capsule Preparation: PLGA was dissolved into 4 mL methylene chloride with the desired amount of liquid PFOB and placed in a thermostated bath maintained at 20 °C to ensure full miscibility of the PFOB. The organic solution was then emulsified into 20 mL of 1.5% sodium cholate w/v aqueous solution using an Ultra-turrax T25 (IKA-Labortechnik, Staufen, Germany) operating with an SN25-10G dispersing tool at a velocity between 8000 and 24 500 rpm. Emulsification was performed in a 50 mL beaker placed over ice for 2 min. Methylene chloride was then evaporated by magnetic stirring for about 3 h at 300 rpm in a thermostated bath (20 °C). For fluorescent or confocal microscopy, Nile Red was added to the organic solution prior to emulsification. Typically, about 100 μL of a concentrated Nile Red solution (0.057 mg mL^{-1} in methylene chloride) was added to the organic solution prior to emulsification.

To further decrease the capsule size and obtain nanocapsules, a pre-emulsion was prepared by mixing both the organic and aqueous phases with an Ultra-turrax at 8000 rpm for 30 s. The pre-emulsion was then sonicated with a vibrating metallic tip Vibra cell (Bioblock Scientific, France), for 2 min over ice. The variation of sonication power is expressed as a function of the applied voltage. The voltage range was between 40 and 140 V. The rest of the process is similar to the one described for microcapsules. Fresh capsules were optionally frozen at −20 °C after addition of PVA [final concentration 0.2% (w/v)] used as a cryoprotectant [41], and then freeze-dried for 24–48 h using a LYOVAC GT2 (Leybold-Heraeus, Köln, Germany).

Microscopy Techniques: For regular microscopy, we use a Leitz Diaplan microscope equipped with a Coolsnap ES camera (Roper Scientific) and for confocal microscopy, a Zeiss LSM-510 confocal scanning laser microscope equipped with a 1 mW Helium Neon laser) using a Plan Apochromat 63X objective (NA 1.40, oil immersion). The pinhole diameter was set at 71 μm. Stacks of images were collected every 0.42 μm along the *z*-axis. Fluorescent samples dyed with Nile Red were excited at 543 nm and observed at 560 nm. Scanning electron microscopy (SEM) was performed using a LEO 1530 (LEO Electron Microscopy, Inc., Thornwood, NY) operating between 1 and 3 kV with a filament current of about 0.5 mA. Liquid samples were deposited on carbon conductive double-sided tape (Euromedex, France) and dried at room temperature. They were coated with a palladium–platinum layer of about 4 nm using a Cressington sputter-coater 208HR with a rotary-planetary-tilt stage, equipped with an MTM-20 thickness controller. Particles were washed before imaging by centrifugation to remove the excess of surfactant that reduces the quality of images. Transmission electron microscopy (TEM) was performed using a Philips EM208 operating at 80 kV. Suspensions of nanocapsules were deposited on copper grids covered with a formwar film (400-mesh) for 2 min. The excess solution was blotted off using filter paper and grids were air-dried before observation. Images were acquired using a high-resolution camera Advantage HR3/12GO4 (AMT-Hamamatsu).

Size Measurements: Size measurements on microcapsules were performed using an LS230 Coulter-Beckmann granulometer based on laser diffraction. Drops of the capsules suspension were added to water in the measurement cuvette. Measurements were performed in triplicate. Size distribution was analyzed using either the Fraunhoffer model or the Mie model, according to the size observed with microscopy. Size measurements on nanocapsules were performed using a Malvern Zetasizer Nano ZS based on quasi-elastic light scattering. Measurements were performed in triplicate at an angle of 173 ° to avoid multiple scattering.

In Vitro Ultrasound Measurements: Capsule suspensions were placed in a 3-mm deep, cylindrical, stainless steel chamber. The top of the chamber was sealed with an acoustically transparent cellophane membrane. At its bottom, a small 1-mm-deep cylindrical cavity allowed a magnetic stir bar to agitate the suspension. The chamber was immersed in water and insonified along an axis perpendicular to the cellophane membrane using a 50 MHz polyvinylidene fluoride broadband transducer (model PI 75-1, Panametrics, Inc., USA) positioned so that its focus was approximately 1 mm beyond the echo from the cellophane membrane, within the solution. During the experiment, the transducer emitted ultrasound pulses at a repetition rate of 1 kHz using a Panametrics Sofranel 5900 PR emitter/receiver. The pulse duration was 0.08 μs at −20 dB of the negative peak value, and the −6 dB band pass ranged from 40 to 60 MHz. The backscattered ultrasound signal was received by the same transducer, digitized at a sampling rate of 400 MHz on a digital oscilloscope (model 9450A, Lecroy, USA) and transferred to a personal computer for signal processing using MATLAB©. A fast Fourier transform was performed on the signal in a 530-point (1.98 mm) Hamming window beginning at the position of the transducer focus. Experiments were performed for both the capsule suspensions and the solvent, the latter giving a reference for the noise level. Finally, the SNR, which measures the contrast enhancement, was derived over an average of 15 measurements.

Stability Experiments: To assess capsule stability, freeze-dried capsules were reconstituted in PBS (pH 7.4) and incubated at 37 °C with stirring. Capsule size distribution was measured at several time points using light scattering for nanocapsules and granulometry for microcapsules. Microcapsules were also imaged using fluorescent microscopy at several time points. In addition, the ultrasound contrast stability (40–60 MHz) was evaluated by measuring the SNR (40–60 MHz) as described above for a 50 mg mL^{-1} suspension of 6 μm capsules and of a 50 mg mL^{-1} suspension of nanocapsules over a 20-min period.

Volumetric and Compressibility Measurements: We first derived the specific volume, v^0, of nanocapsules using the well-known relationship: $v^0 = 1/\rho_0 - (\rho - \rho_0)/(\rho_0 c)$, where c is the nanocapsule concentration, ρ and ρ_0 are the densities of the nanocapsule suspension and of the solvent, respectively [measured with a precision of $\pm 1.5 \times 10^{-4}$% using a DMA 58 vibrating tube densimeter (Anton Paar, Austria)]. We then derived the specific sound velocity increment: $[u] = (U - U_0)/(U_0 c)$, where U and U_0 are the sound velocities in the suspension and in the solvent, respectively (measured with a precision of at least $<10^{-4}$% using an ultrasound resonator cell with lithium niobate piezotransducers at 7.5 MHz [42, 43]). Finally, the values of $[u]$ and v^0 are used to calculate the specific adiabatic compressibility, k^0_S, of nanocapsules using the following relationship: $k^0_S = \beta_{S0}(2v^0 - 2[u] - 1/\rho_0)$, where β_{S0} is the coefficient of adiabatic compressibility of the solvent [44,45].

In Vitro Ultrasound Imaging: Capsules suspensions were sonicated for 1 min before injection in a silicone tube placed in a room-temperature water bath such that tube's posterior wall was at the focal zone of a broadband 7–14 MHz, clinical ultrasound probe (Sonoline Elegra, Siemens, Germany). Images of the contrast suspension were obtained in both normal mode (center transmit frequency ∼9 MHz) and in a pulse-inversion imaging mode (THI, Ensemble Contrast Imaging™, center transmit frequency ∼9 MHz). The transmit power was 100% of the system maximum which corresponds to a theoretical mechanical index of 1. The receiver gain was set to 60 dB and the time gain compensation settings were fixed in a median position. The dynamic range was 65 dB with a linear display curve.

In Vivo Ultrasound Imaging: Animals use procedures were in accordance with the recommendations of the EEC (86/609/CEE) and the French National Committee (decree 87/848) for the care and use of laboratory animals. Three male NMRI-nu (nu/nu) mice weighing from 26 to 31 g (Elevage Janvier, Le Genest-St-Isle, France) were imaged.

Anesthesia was performed by intra-peritoneal injection of 180 μL of ketamine/xylazine/physiological serum solution (20:10:70 v/v/v). *In vivo* ultrasound imaging was performed using a Toshiba Aplio clinical imaging system in THI mode (18 fps) with a broadband 7–14 MHz probe at a mechanical index of 1.6. The receiver gain and the time gain compensation settings were selected to obtain homogenous brightness throughout the imaged depth. The dynamic range was 65 dB with a linear display curve. After initial setting, these parameters were not changed throughout the series of imaging trials. In an image plane presenting the liver and the inferior vena cava, a 60-s long image-sequence acquisition was initiated just prior to agent injection. A 200-μL dose of nanocapsule suspension (150 nm, 50 mg mL^{-1}, $T/R = 0.35$) was injected intravenously. Thus, the sequence includes baseline and bolus passage. Images were then acquired approximately every 2 min up to 30 min after agent injection.

^{19}F NMR Spectroscopy and MRI: ^{19}F nuclear magnetic resonance (NMR) spectra were recorded on a Bruker 400 Avance Instrument (Karlsruhe, Germany) working at 9.4T at room temperature, with D_2O as an internal standard and a dual ^{19}F-^{1}H probe. The SNR was measured as a function of capsule concentration (150 nm, $T/R = 0.35$) on the CF_3 peak using Bruker's sino function. T1 measurements were performed on pure PFOB and PFOB nanocapsules using a Bruker's pulse sequence (t1ir) based on inversion recovery.

MRI experiments were carried out on a 9.4T vertical wide-bore spectrometer (Bruker 400 Avance). The magnet was equipped with a 950 mT m^{-1} gradient coil and Paravision 4.0 acquisition/processing software. Experiments were carried out with a $^{1}H/^{19}F$ 12 mm inner diameter custom-made copper loop-gap coil: ^{19}F (376.5 MHz) and ^{1}H (400.13 MHz). First, in order to verify the sensitivity of the measurement 1D ^{19}F NMR nonlocalized spectra were recorded: 54 000 Hz spectral width and one average. The NMR spectrum of PFOB presents several resonance peaks related to its chemical structure. Therefore the classical MRI image will present chemical shifts artifacts. These artifacts were avoided using a frequency selective pulse centered on the CF_3 frequency. ^{19}F spin echo images were obtained with a 2D CHESS sequence, using a Gaussian excitation pulse (2480 Hz bandwidth) and a 5 ms echo time. Gradient echo images were obtained with a GE3D sequence using the same excitation pulse. The flip angle of this pulse was related to the repetition time and T1 by the Ernst relation to optimize sensitivity and a 1.6 ms echo time was used. In both cases, a $2 \times 2\,cm^2$ FOV was used with an acquisition matrix of 32×32 (or 64×64) and the size in the third dimension was 3 mm. Evaluation of the apparent T2 of the CF_3 signal was made with PRESS sequence using selective pulses in a centered voxel of $3 \times 3 \times 3$ mm^3. Samples of pure PFOB and 50 mg mL^{-1} PFOB nanocapsules in water (150 nm, $T/R = 0.35$) were observed.

Received: April 1, 2008
Revised: May 26, 2008
Published online:

[1] H. Schoder, S. C. Ong, *Semin. Nucl. Med.* **2008**, *38*, 119.
[2] M. Hughes, S. Caruthers, T. Tran, J. Marsh, K. Wallace, T. Cyrus, K. Partlow, M. Scott, M. Lijowski, A. Neubauer, P. Winter, G. Hu, H. Zhang, J. McCarthy, B. Maurizi, J. Allen, C. Caradine, R. Neumann, J. Arbeit, G. Lanza, S. Wickline, *Proc. IEEE* **2008**, *96*, 397.
[3] C. P. Slichter, *Principles of Magnetic Resonance*, Springer, Berlin **1996**.
[4] M. H. Rapacholi, *Essentials of Medical Ultrasound*, Humana press, New York **1982**.
[5] G. Renault, P. Bonnin, C. Marchiol-Fournigault, J. M. Gregoire, S. Serriere, B. Richard, D. Fradelizi, *J. Radiol.* **2006**, *87*, 1937.
[6] D. G. Norris, *J. Magn. Reson. Imag.* **2003**, *18*, 519.
[7] J. A. Straub, D. E. Chickering, C. C. Church, B. Shah, T. Hanlon, H. Bernstein, *J. Control. Release* **2005**, *108*, 21.
[8] W. Cui, J. Bei, S. Wang, G. Zhi, Y. Zhao, X. Zhou, H. Zhang, Y. Xu, *J. Biomed. Mater. Res. B: Appl. Biomater.* **2005**, *73*, 171.
[9] D. M. El-Sherif, M. A. Wheatley, *J. Biomed. Mater. Res. A* **2003**, *66*, 347.
[10] D. M. El-Sherif, J. D. Lathia, N. T. Le, M. A. Wheatley, *J. Biomed. Mater. Res. A* **2004**, *68*, 71.
[11] S. C. Quay, *J. Ultrasound Med.* **1994**, *13*, S9.
[12] G. M. Lanza, K. D. Wallace, M. J. Scott, W. P. Cacheris, D. R. Abendschein, D. H. Christy, A. M. Sharkey, J. G. Miller, P. J. Gaffney, S. A. Wickline, *Circulation* **1996**, *94*, 3334.
[13] S. A. Wickline, M. Hughes, F. C. Ngo, C. S. Hall, J. N. Marsh, P. A. Brown, J. S. Allen, M. D. McLean, M. J. Scott, R. W. Fuhrhop, G. M. Lanza, *Acad. Radiol.* **2002**, *9*, S290.
[14] R. F. Code, J. E. Harrison, K. G. Mcneill, M. Szyjkowski, *Magn. Reson. Med.* **1990**, *13*, 358.
[15] G. M. Lanza, P. M. Winter, A. M. Neubauer, S. D. Caruthers, F. D. Hockett, S. A. Wickline, *Curr. Top. Dev. Biol.* **2005**, *70*, 57.
[16] X. B. Fan, J. N. River, A. S. Muresan, C. Popescu, M. Zamora, R. M. Culp, G. S. Karczmar, *Phys. Med. Biol.* **2006**, *51*, 211.
[17] U. Wolf, A. Scholz, C. P. Heussel, K. Markstaller, W. G. Schreiber, *Magn. Reson. Med.* **2006**, *55*, 948.
[18] E. T. Ahrens, R. Flores, H. Y. Xu, P. A. Morel, *Nat. Biotechnol.* **2005**, *23*, 983.
[19] U. Noth, S. P. Morrissey, R. Deichmann, H. Adolf, C. Schwarzbauer, J. Lutz, A. Haase, *Magn. Reson. Med.* **1995**, *34*, 738.
[20] F. A. Bovey, *Nuclear Magnetic Resonance Secptroscopy*, Academic Press, San Diego **1988**.
[21] A. M. Reed, D. K. Gilding, *Polymer* **1981**, *22*, 494.
[22] K. Yamaguchi, J. M. Anderson, *J. Control. Release* **1993**, *24*, 81.
[23] M. Andre, T. Nelson, R. Mattrey, *Invest. Radiol.* **1990**, *25*, 983.
[24] E. Pisani, N. Tsapis, J. Paris, V. Nicolas, L. Cattel, E. Fattal, *Langmuir* **2006**, *22*, 4397.
[25] A. Loxley, B. Vincent, *J. Colloid Interface Sci.* **1998**, *208*, 49.
[26] P. T. Leese, R. J. Noveck, J. S. Shorr, C. M. Woods, K. E. Flaim, P. E. Keipert, *Anesth. Analg.* **2000**, *91*, 804.
[27] R. J. Noveck, E. J. Shannon, P. T. Leese, J. S. Shorr, K. E. Flaim, P. E. Keipert, C. M. Woods, *Anesth. Analg.* **2000**, *91*, 812.
[28] F. Forsberg, J. D. Lathia, D. A. Merton, J. B. Liu, N. T. Le, B. B. Goldberg, M. A. Wheatley, *Ultrasound Med. Biol.* **2004**, *30*, 1281.
[29] K. Sarkar, W. T. Shi, D. Chatterjee, F. Forsberg, *J. Acoust. Soc. Am.* **2005**, *118*, 539.
[30] S. Hilgenfeldt, D. Lohse, M. Zomack, *Eur. Phys. J. B* **1998**, *4*, 247.
[31] N. de Jong, A. Bouakaz, P. Frinking, *Echocardiography* **2002**, *19*, 229.
[32] J. S. Allen, D. E. Kruse, K. W. Ferrara, *IEEE Trans. Ultrason. Ferroelectr. Freq. Control* **2001**, *48*, 409.
[33] J. S. Allen, D. J. May, K. W. Ferrara, *Ultrasound Med. Biol.* **2002**, *28*, 805.
[34] J. N. Marsh, C. S. Hall, M. J. Scott, R. W. Fuhrhop, P. J. Gaffney, S. A. Wickline, G. M. Lanza, *IEEE Trans. Ultrason. Ferroelectr. Freq. Control* **2002**, *49*, 29.
[35] O. Couture, P. D. Bevan, E. Cherin, K. Cheung, P. N. Burns, F. S. Foster, *Ultrasound Med. Biol.* **2006**, *32*, 73.
[36] O. Couture, P. D. Bevan, E. Cherin, K. Cheung, P. N. Burns, F. S. Foster, *Ultrasound Med. Biol.* **2006**, *32*, 1247.
[37] D. M. El-Sherif, J. D. Lathia, N. T. Le, M. A. Wheatley, *J. Biomed. Mater. Res. A* **2004**, *68*, 71.
[38] D. M. El-Sherif, M. A. Wheatley, *J. Biomed. Mater. Res. A* **2003**, *66*, 347.

ADVANCED FUNCTIONAL MATERIALS

[39] R. Gref, Y. Minamitake, M. T. Peracchia, V. Trubetskoy, V. Torchilin, R. Langer, *Science* **1994**, *263*, 1600.
[40] M. S. Hughes, J. N. Marsh, C. S. Hall, R. W. Fuhrhop, E. K. Lacy, G. M. Lanza, S. A. Wickline, *J. Acoust. Soc. Am.* **2005**, *117*, 964.
[41] W. Abdelwahed, G. Degobert, H. Fessi, *Int. J. Pharm.* **2006**, *309*, 178.
[42] F. Eggers, *Acustica* **1992**, *76*, 231.
[43] F. Eggers, U. Kaatze, *Meas. Sci. Technol.* **1996**, *7*, 1.
[44] B. B. Owen, H. L. Simons, *J. Phys. Chem.* **1957**, *61*, 479.
[45] A. P. Sarvazyan, *Ann. Rev. Biophys. Biophys. Chem.* **1991**, *20*, 321.